International Journal for Modern Trends in Science and Technology
Volume 12, Issue 04, pages 787-797
ISSN: 2455-3778 online
Available online at: http://www.ijmtst.com/vol12issue04.html
DOI: https://doi.org/10.5281/zenodo.19567917

Power Quality Improvement using SEPIC–ĆUK Based Bipolar DC-Link Transformerless Inverter for Grid-Connected PV System

Dr.B.Srinivasa Raju, T.Navya, Sk.Reshma, V.Krishnaveni, S.Naga Rajesh

Department of Electrical and Electronics Engineering, Vasireddy Venkatadri Institute of Technology, Pedakakani, Namburu, Guntur, India.

To Cite this Article
Dr.B.Srinivasa Raju, T.Navya, Sk.Reshma, V.Krishnaveni & S.Naga Rajesh (2026). Power Quality Improvement using SEPIC–ĆUK Based Bipolar DC-Link Transformerless Inverter for Grid-Connected PV System. International Journal for Modern Trends in Science and Technology, 12(04), 787-797. https://doi.org/10.5281/zenodo.19567917

Article Info
Received: 16 March 2026; Revised: 06 April 2026; Accepted: 10 April 2026.

KEYWORDS

Photovoltaic (PV) system, power quality improvement, SEPIC–Ćuk converter, bipolar DC-link, transformerless inverter, grid-connected system, total harmonic distortion (THD), maximum power point tracking (MPPT).

ABSTRACT

The increasing penetration of photovoltaic (PV) systems into the electrical grid introduces significant challenges related to power quality, efficiency, and system reliability. This paper presents a novel approach for power quality improvement using a SEPIC–Ćuk based bipolar DC-link integrated with a transformerless inverter for grid-connected PV applications. The proposed topology combines the advantages of SEPIC and Ćuk converters to achieve both step-up and step-down voltage conversion with reduced ripple and improved voltage regulation. The bipolar DC-link structure enables balanced voltage distribution, minimizes common-mode leakage currents, and enhances the overall safety of transformerless operation. Additionally, the elimination of the transformer reduces system cost, size, and losses, thereby improving efficiency. The proposed system effectively mitigates power quality issues such as voltage fluctuations, harmonic distortion, and poor power factor. A suitable control strategy is implemented to ensure maximum power point tracking (MPPT) and stable grid synchronization. The performance of the system is validated through simulation results, demonstrating improved total harmonic distortion (THD), enhanced power factor, and reliable operation under varying solar irradiance conditions. The results confirm that the proposed SEPIC–Ćuk based bipolar DC-link inverter is an efficient and cost-effective solution for enhancing power quality in grid-connected photovoltaic systems.

1. INTRODUCTION

The global transition toward clean and sustainable energy systems has significantly accelerated the deployment of photovoltaic (PV) generation technologies in both residential and utility-scale applications. Among various renewable sources, solar PV has emerged as one of the most promising due to its scalability, environmental friendliness, and declining installation costs [1], [2]. As PV penetration increases within modern power grids, it introduces several operational and technical challenges, particularly in terms of power quality, system stability, and grid compatibility [3], [4]. Unlike conventional synchronous generators, PV systems are inherently intermittent and depend on environmental conditions such as solar irradiance and temperature, leading to fluctuations in output power and voltage levels [5]. One of the most critical components in a grid-connected PV system is the power electronic interface, typically consisting of DC–DC converters and DC–AC inverters. These components are responsible for conditioning the generated power and ensuring that it meets grid standards before injection into the utility network [6]. However, improper design or control of these converters can result in significant power quality issues, including harmonic distortion, voltage fluctuations, reactive power imbalance, and poor power factor [3], [7]. These issues not only affect the performance of the PV system but also deteriorate the overall grid stability and efficiency. In recent years, transformerless inverter topologies have gained widespread attention due to their advantages over traditional transformer-based systems. The elimination of the transformer reduces system cost, volume, and weight while improving efficiency by minimizing conduction and core losses [8], [9]. Despite these advantages, transformerless systems introduce challenges such as common-mode (CM) leakage currents, which arise due to the parasitic capacitance between the PV array and the ground [10]. These leakage currents can lead to safety hazards, electromagnetic interference (EMI), and degradation of power quality [11]. Therefore, mitigating leakage current while maintaining high efficiency remains a key research focus in transformerless PV systems. To address these challenges, various inverter topologies such as H5, HERIC, and neutral-point clamped (NPC) structures have been proposed [12], [13]. While these configurations improve leakage current performance, they often involve increased circuit complexity or switching losses. An alternative approach involves modifying the DC-link structure itself. In particular, the bipolar DC-link configuration has shown promising potential in reducing common-mode voltage variations and achieving balanced voltage distribution across the inverter terminals [14]. This not only enhances safety but also contributes to improved harmonic performance and reduced leakage current. Another important aspect of PV system design is the DC–DC conversion stage, which is essential for voltage regulation and maximum power extraction. Conventional converters such as buck, boost, and buck–boost converters have limitations in handling wide input voltage variations and achieving low ripple output [15]. In this context, SEPIC (Single-Ended Primary Inductor Converter) and Ćuk converters have gained attention due to their ability to provide both step-up and step-down voltage conversion while maintaining continuous input and output current [16], [17]. The SEPIC converter is known for its non-inverting output and low input current ripple, making it suitable for PV applications where smooth current flow is desirable [16]. On the other hand, the Ćuk converter offers low output current ripple and improved energy transfer efficiency through capacitive coupling [17]. Recent research has explored the integration of SEPIC and Ćuk converters to combine their advantages and overcome individual limitations. The hybrid SEPIC–Ćuk topology enables enhanced voltage regulation, reduced ripple content, and improved dynamic response under varying solar conditions [18], [19]. Additionally, such integrated converters can provide better electromagnetic compatibility and reduced stress on switching devices, thereby improving overall system reliability. Another critical requirement in grid-connected PV systems is the implementation of Maximum Power Point Tracking (MPPT) algorithms. MPPT techniques such as Perturb and Observe (P&O), Incremental Conductance (IC), and fuzzy logic-based methods are widely used to ensure that the PV array operates at its maximum power point under varying environmental conditions [20]. Efficient MPPT control not only maximizes energy extraction but also stabilizes the DC-link voltage, which is essential for proper inverter operation. In addition to MPPT, grid synchronization and control strategies play a crucial role in ensuring seamless integration of PV systems with the

utility grid. Techniques such as phase-locked loops (PLL), current control methods, and voltage-oriented control are commonly employed to maintain synchronization and regulate power flow [21]. Proper control strategies help in reducing total harmonic distortion (THD), improving power factor, and ensuring compliance with grid standards. Despite significant advancements in PV inverter technologies, achieving an optimal balance between efficiency, cost, and power quality remains a challenging task. Existing solutions often involve trade-offs between complexity and performance. Therefore, there is a need for innovative topologies that can simultaneously address voltage regulation, harmonic mitigation, leakage current suppression, and system efficiency. In this context, the present work proposes a SEPIC–Ćuk based bipolar DC-link integrated with a transformerless inverter for grid-connected PV applications. The proposed system combines the advantages of hybrid DC–DC conversion and bipolar DC-link architecture to enhance power quality and operational reliability. The integration of SEPIC and Ćuk converters ensures flexible voltage conversion with reduced ripple, while the bipolar DC-link structure minimizes common-mode voltage and leakage current issues. Furthermore, the transformerless inverter configuration improves efficiency by eliminating bulky magnetic components. The proposed system also incorporates an effective control strategy that includes MPPT for maximum energy extraction and grid synchronization for stable power injection. The overall objective is to improve key performance metrics such as total harmonic distortion (THD), power factor, voltage stability, and efficiency under varying solar irradiance conditions. The remainder of this paper presents the detailed design, modeling, control strategy, and simulation analysis of the proposed system. The results demonstrate that the SEPIC–Ćuk based bipolar DC-link inverter provides a robust, efficient, and cost-effective solution for enhancing power quality in grid-connected PV systems.

II. System Configuration

The proposed system consists of a SEPIC–Ćuk based bipolar DC-link integrated with a transformerless inverter for grid-connected photovoltaic (PV) applications. It includes a PV source, hybrid SEPIC–Ćuk DC–DC converter, bipolar DC-link, three-phase inverter, LCL filter, and grid interface. The PV array generates DC power under varying environmental conditions, and a Maximum Power Point Tracking (MPPT) algorithm ensures maximum energy extraction by generating the duty cycle for the converter switch. The DC–DC stage employs a hybrid SEPIC–Ćuk converter, combining the advantages of both topologies to achieve step-up/step-down voltage conversion with reduced ripple and improved regulation. The SEPIC section provides continuous input current, while the Ćuk section ensures low output ripple. This integration enhances performance and dynamic response. The converter output feeds a bipolar DC-link formed by capacitors that split the voltage into two balanced levels. This structure provides a neutral midpoint and reduces common-mode voltage, thereby minimizing leakage current in transformerless operation and improving system safety and performance. A voltage controller maintains DC-link stability. The DC-link supplies a three-phase voltage source inverter (VSI), which converts DC power into AC using sinusoidal PWM. The control strategy is based on the dq reference frame to regulate inverter currents and control power flow. An LCL filter is used at the inverter output to reduce harmonics and ensure a near-sinusoidal current waveform. A phase-locked loop (PLL) is used for grid synchronization, providing the necessary phase angle for control. The current controller regulates active and reactive power while maintaining low THD and high power factor. Overall, the system ensures efficient power conversion, improved power quality, reduced leakage current, and reliable grid integration.

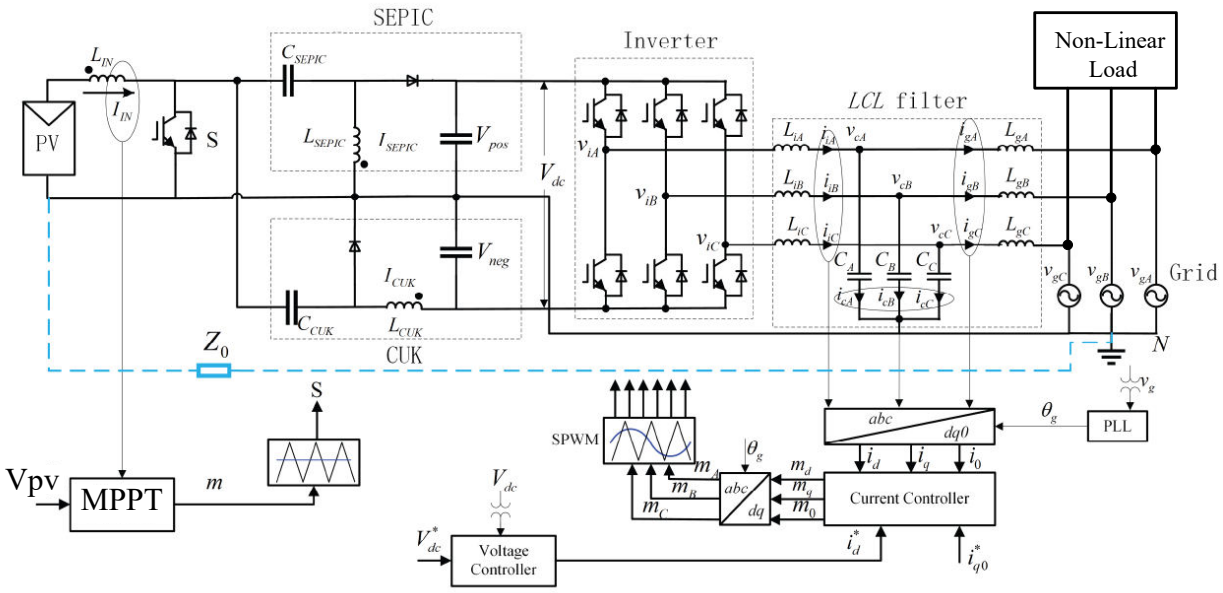

Fig. 1. Proposed SEPIC–Ćuk Based Bipolar DC-Link - Transformerless Inverter for Grid-Connected PV System

III. Proposed System Designing

A. Solar Photovoltaic Panel Modeling

Here, we lay out the basic idea for a hybrid renewable energy system using the PV model. Here, we zero in on the PV cell type seen in Fig. 2 that has a single diode. For a depiction of the equivalent circuit of a solar PV panel using a single diode, refer to Figure 2.

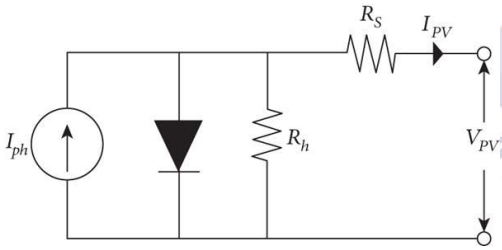

Figure 2 Equivalent circuit of PV panel.

As shown in equation (1), a PV panel's output current may be calculated.

$$I_{PV} = N_P I_{Ph} - N_P I_o \left(exp\left[\frac{q\left(V_{PV}/N_s + I_{PV}R_s/N_P\right)}{nkT}\right] - 1\right) - \frac{V_{PV}+I_{PV}R_s}{R_h} \quad (1)$$

This is where the following symbols are defined: V_{PV}, which stands for the voltage generated by the PV panel; I_o, for output current; I_{Ph}, for input current; and I_{PV}, for input current from the light source. R_h and R_s are the shunt and series resistances, respectively. N_P stands for the total number of cells linked in parallel, whereas N_s represents the number of cells linked in serial. The ideal diode has a value of 1, and the variables K, T, q, and n stand for Boltzmann's constant, the temperature of the PV panel, the charge on an electron, and the ideality of the diode, respectively ($1 \cdot 602 \times 10^{-19}C$, $1.38 \times 10^{-23}J$ / k),. The temperature of the PV panel influences both Io and (I_{Ph}), while irradiance (G) only influences the light generated current (I_{Ph}). Eq. (2) shows how temperature affects the reverse saturation current (I_o), and Eq. (3) shows how temperature and irradiance affect the light-generated current [17]. For further information on how to simulate PV arrays, see [17].

$$I_0 = I_{0,n}\left(\frac{T_n}{T}\right)^3 exp\left(\frac{qEgo}{nk}\left(\frac{1}{T_n} - \frac{1}{T}\right)\right) \quad (2)$$

$$I_{Ph} = \left(I_{Ph,n} + k_1(T - T_n)\right)\frac{G}{G_n} \quad (3)$$

The following variables are defined: T_n = 25°C, Gn = 1000 watts/sq. m., I_o ,n = saturation current, I_{Ph} ,n = light current, E_{go} = energy across the bandgap of the solar cell, and k_1 = reference temperature coefficient for a short circuit.

B. Characteristics of Solar PV Panel

We may deduce from equations (1)–(3) that (i) the relationship between Ipv and Vpv is not linear, (ii) the I–V characteristics of the solar cell are substantially affected by the diode in the same circuit, and (iii) this nonlinearity is rather large. We model the I-V and P-V characteristics at two irradiance levels and temperatures, maintaining one parameter at its STH value and altering the other, to investigate the impact of these two factors. Figure 3 displays the simulated current-voltage and current-polarity characteristics for 500 W/m^2 and 1000 W/m^2 irradiance at a constant 25°C. Open-circuit voltage is not linear with respect to irradiance, but short-circuit current is. Consequently, the maximum

achievable power production is roughly proportional to the irradiation.

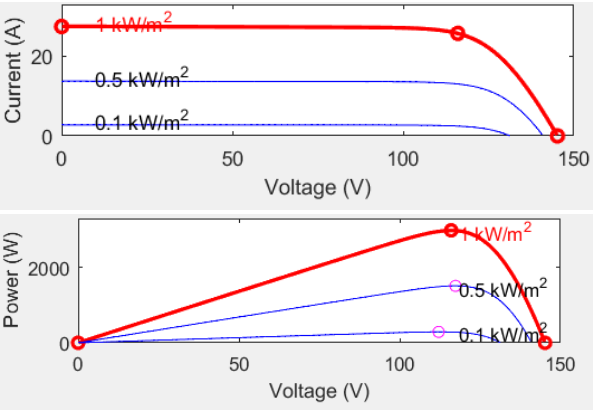

Figure 3 I-V and P-V characteristics of a PV panel.

Shadows Solar panels don't work well in situations where they're shaded, which happens often due to things like clouds, trees, birds, and buildings [17]. This emphasises the need of effective power management systems that can adjust to situations with partial shade. So, to lessen the impact of partial shade, it could be necessary to use extra measures like bypass diodes. The proposed PVE was conceived as a model of the reaction of a PV panel to two different levels of irradiance at the same time. To find out what a partly shaded PV panel is like, we keep the temperature constant at 25°C and expose the unshaded cells to 1000 W/m^2, while the shaded cells get 300 W/m^2.

TABLE 1. Parameter Specifications of BP Solar 1Soltech 1STH-215-P PV Module

Description	Ratings
Maximum power (PMP)	213.15 W
Maximum current (IMP)	7.35 A
Maximum voltage (VMP)	29 V
Short circuit current (ISC)	7.84 A
Temperature (T)	25^0C
Open circuit voltage (Voc)	36.3 V
Parallel strings	3.5
Series-connected modules per string	4
Solar irradiation (G)	1000W/m2

C. *SOLAR ENERGY CONVERSION SYSTEM (SECS)*

Solar photovoltaic panels, a DC-DC boost converter, and a maximum power point tracking (MPPT) controller make up the SECS. Whether the MPPT is in standby or active mode depends on the battery storage system's charge level. A solar PV panel's voltage and current output are constantly monitored by the MPPT controller. It optimises the DC-DC boost converter's working point to transmit solar power to the batteries as efficiently as possible. This guarantees that the battery is charged efficiently and that solar energy is used to its fullest potential.

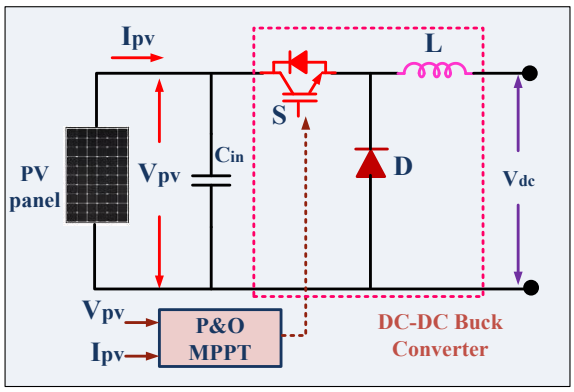

Fig. 4 solar PV P&O MPPT DC-DC Buck converter

D. Perturbation and observation (P&O)

The voltage is optimised in real time using this technique. A basic P&O MPPT algorithm is provided below as an example, while there are more complex and efficient variants of this method. In order to keep the PV system operating at, or close to, the peak power point of the PV panel regardless of environmental factors like changing solar irradiance, temperature, and load, maximum power point tracking (MPPT) is an algorithm built into photovoltaic (PV) inverters. Engineers creating solar converters use P&O MPPT algorithms to optimise PV system output. As a result of the algorithms' manipulation of the voltage, the system is kept at its "maximum power point" (peak voltage) along the power voltage curve at all times. Controller designs for PV systems often use MPPT algorithms.

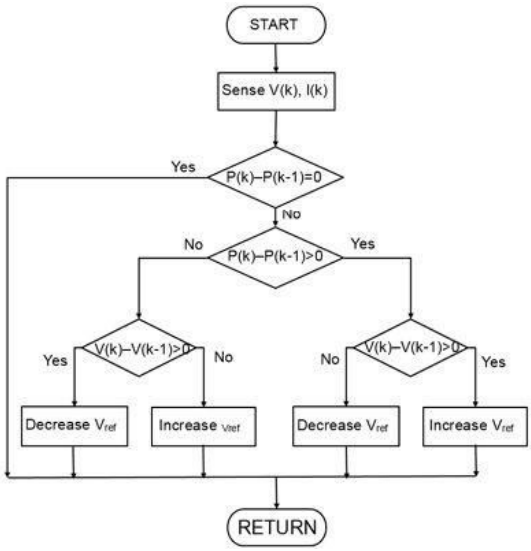

Fig .5 The perturb and observe algorithm flow chart for a solar DC-DC converter.

In order to keep the PV system producing as much electricity as possible, the algorithms take into consideration variables outside of the system, such as temperature and changing irradiance (sunlight).

IV. Working and Operation of Proposed SEPIC–Ćuk Converter

The proposed SEPIC–Ćuk converter is a hybrid DC–DC topology formed by combining the SEPIC and Ćuk converters to generate a bipolar DC output with both positive and negative voltage levels from a single DC source. This configuration uses a common switch S, shared input inductor, and a common ground, which simplifies the circuit while improving efficiency and control. The SEPIC section produces a positive output voltage Vpos, while the Ćuk section generates a negative output voltage Vneg, enabling the formation of a bipolar DC-link suitable for inverter applications. The operation of the converter can be explained in two switching modes. When the switch S is ON, the input inductor Lin stores energy from the source, and both SEPIC and Ćuk inductors LSEPIC and LCUK) are energized. During this interval, the diodes are reverse biased, and the capacitors CSEPIC and CCUK transfer energy within their respective sections. The inductor voltages during the ON state can be expressed as

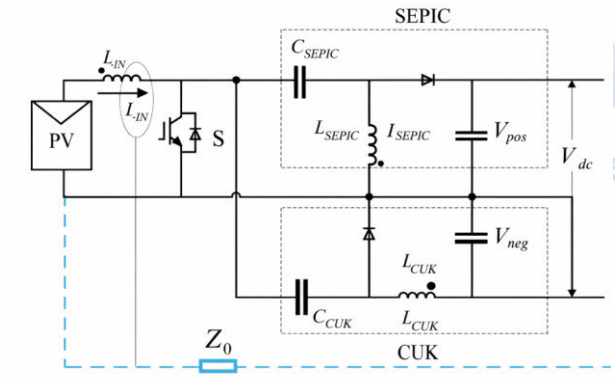

Fig.6 Combined SEPIC-CUK Converter topology

$$V_{L_{in}} = V_g \quad (3)$$

$$V_{L_{SEPIC}} = V_g \quad (4)$$

$$V_{L_{CUK}} = -V_g \quad (5)$$

When the switch S is OFF, the stored energy in the inductors is released to the output through the diodes. The SEPIC section supplies energy to the positive output capacitor, while the Ćuk section delivers energy to the negative output capacitor. In this mode, the inductor voltages become

$$V_{L_{in}} = V_g - V_O \quad (6)$$

$$V_{L_{SEPIC}} = V_g - V_{pos} \quad (7)$$

$$V_{L_{CUK}} = V_g - V_{neg} \quad (8)$$

Assuming ideal components and applying the volt–second balance principle on inductors under continuous conduction mode (CCM), the output voltage relation for both SEPIC and Ćuk sections is obtained as

$$V_o = \frac{D}{1-D} V_g \quad (9)$$

Thus, the positive and negative outputs are given by

$$V_P = \frac{D}{1-D} V_g \quad (10)$$

$$V_{neg} = -\frac{D}{1-D} V_g \quad (11)$$

This shows that the converter produces equal magnitude but opposite polarity voltages, forming a balanced bipolar DC-link.

The input and output current relationship in CCM is expressed as

$$I_g = I_o \frac{D}{1-D} \quad (12)$$

In discontinuous conduction mode (DCM), the voltage conversion ratio becomes dependent on load and inductance, given by

$$V_o(DCM) = D \cdot V_g \sqrt{\frac{RT_s}{2L_{eq}}} \quad (13)$$

where the equivalent inductance is

$$\frac{1}{L_{eq}} = \frac{1}{L_1} + \frac{1}{L_2} \quad (14)$$

and the condition for DCM operation is

$$\frac{2L_{eq}}{(1-D)^2 RT_s} < 1 \quad (15)$$

The duty cycle D is defined as

$$D = \frac{T_{ON}}{T_s} \quad (16)$$

where TON is the switch ON time and Ts is the switching period.

Overall, the proposed SEPIC–Ćuk converter provides non-pulsating input current, reduced ripple, and symmetric bipolar output, making it highly suitable for transformerless inverter applications. The use of a single switch and common ground reduces circuit complexity while enabling efficient power conversion and improved dynamic performance.

V. Control of Bidirectional Grid-Connected AC–DC Voltage Source Converter

The bidirectional grid-connected AC–DC voltage source converter (VSC) is employed to regulate the DC-link voltage and control the exchange of active and reactive

power between the DC side and the utility grid. The converter operates in both rectification and inversion modes, thereby enabling bidirectional power flow depending on the operating condition of the distributed energy source or storage system. In addition, the converter ensures sinusoidal grid currents, low harmonic distortion, and controllable power factor at the point of common coupling (PCC). The control strategy is generally based on the synchronous reference frame (SRF) theory, which enables independent control of active and reactive current components.

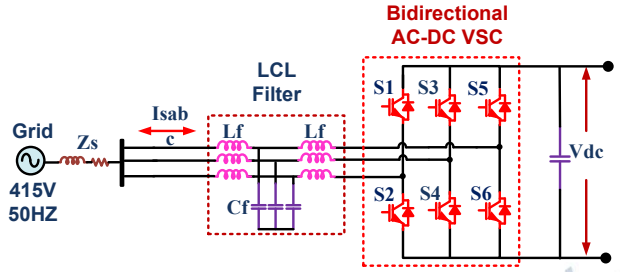

Fig.7 designing of bidirectional AC–DC voltage source converter

Initially, the DC-link voltage Vdc is sensed and compared with its reference value Vdcref. The voltage error is expressed as

$$e(t) = V_{dc}^{ref} - V_{dc} \tag{17}$$

This error is processed through a proportional–integral (PI) controller to generate the reference direct-axis current id∗, which governs the active power transfer between the AC and DC sides:

$$i_d^* = K_p e(t) + K_i \int e(t)\, dt \tag{18}$$

where Kp and Ki are the proportional and integral gains of the DC-link voltage controller. The direct-axis current component controls the active power flow, while the quadrature-axis component controls the reactive power exchanged with the grid.

The three-phase grid currents (ia,ib,ic) are transformed into the synchronous rotating dq reference frame using Park's transformation. The transformation angle θ is obtained through a phase-locked loop (PLL) synchronized with the grid voltage. The transformation is given by

$$\begin{bmatrix} i_d \\ i_q \\ i_0 \end{bmatrix} = \frac{2}{3} \begin{bmatrix} \cos\theta & \cos\left(\theta - \frac{2\pi}{3}\right) & \cos\left(\theta + \frac{2\pi}{3}\right) \\ -\sin\theta & -\sin\left(\theta - \frac{2\pi}{3}\right) & -\sin\left(\theta + \frac{2\pi}{3}\right) \\ \frac{1}{2} & \frac{1}{2} & \frac{1}{2} \end{bmatrix} \begin{bmatrix} i_a \\ i_b \\ i_c \end{bmatrix} \tag{19}$$

In the synchronous reference frame, the fundamental components of the grid currents appear as DC quantities, which simplifies the control design. For unity power factor operation, the reference quadrature-axis current is usually set to zero:

$$i_q^* = 0 \tag{20}$$

If reactive power support is required, then iq∗ can be assigned a nonzero value according to the grid demand. The current errors in the dq frame are then obtained as

$$e_d = i_d^* - i_d \tag{21}$$

$$e_q = i_q^* - i_q \tag{22}$$

These errors are processed through PI current controllers to generate the converter voltage references in the synchronous reference frame. The control equations are expressed as

$$v_d^* = K_{pd} e_d + K_{id} \int e_d\, dt - \omega L i_q + v_d \tag{23}$$

$$v_q^* = K_{pq} e_q + K_{iq} \int e_q\, dt + \omega L i_d + v_q \tag{24}$$

where Kpd, Kid, Kpq, and Kiq are the proportional and integral gains of the current controllers, L is the filter inductance, ω is the angular frequency of the grid, and vd and vq are the grid voltage components in the synchronous frame. The cross-coupling terms ωLiq and ωLid are included to achieve decoupled control of active and reactive currents.

The reference voltages (vd∗,vq∗) are then transformed back into the three-phase stationary frame using the inverse Park transformation:

$$\begin{bmatrix} v_a^* \\ v_b^* \\ v_c^* \end{bmatrix} = \begin{bmatrix} \cos\theta & -\sin\theta & 1 \\ \cos\left(\theta - \frac{2\pi}{3}\right) & -\sin\left(\theta - \frac{2\pi}{3}\right) & 1 \\ \cos\left(\theta + \frac{2\pi}{3}\right) & -\sin\left(\theta + \frac{2\pi}{3}\right) & 1 \end{bmatrix} \begin{bmatrix} v_d^* \\ v_q^* \\ v_0^* \end{bmatrix} \tag{25}$$

These three-phase voltage references are supplied to a sinusoidal pulse width modulation (SPWM) or space vector pulse width modulation (SVPWM) block, which generates the gate pulses for the six switches of the bidirectional VSC. The modulation signals ensure that the converter tracks the desired current references accurately and injects balanced sinusoidal currents into the grid.

The active and reactive powers exchanged between the converter and the grid in the synchronous reference frame are expressed as

$$P = \frac{3}{2}(v_d i_d + v_q i_q) \tag{26}$$

$$Q = \frac{3}{2}(v_q i_d - v_d i_q) \tag{27}$$

When the synchronous frame is aligned with the grid voltage vector, the quadrature component of grid voltage becomes zero, i.e., vq=0, and the power equations reduce to

$$P = \frac{3}{2} v_d i_d \tag{28}$$

$$Q = -\frac{3}{2} v_d i_q \tag{29}$$

From these relations, it is evident that the direct-axis current id controls active power flow and DC-link regulation, while the quadrature-axis current iq controls reactive power exchange. Hence, by appropriately controlling id and iq, the converter can operate bidirectionally, either drawing power from the grid to support the DC bus or injecting power from the DC side into the utility network. In rectification mode, the converter absorbs active power from the AC grid and transfers it to the DC-link, thereby maintaining the required DC voltage for downstream loads or energy storage devices. In inversion mode, the converter injects active power from the DC side into the grid while maintaining synchronization and desired power factor. This bidirectional capability makes the VSC highly suitable for renewable energy systems, battery energy storage systems, electric vehicle charging stations, and hybrid microgrids. Overall, the proposed control strategy enables fast dynamic response, accurate DC-link voltage regulation, decoupled active and reactive power control, and low total harmonic distortion in the grid current. As a result, the bidirectional grid-connected AC–DC voltage source converter ensures efficient and stable power transfer under varying operating conditions.

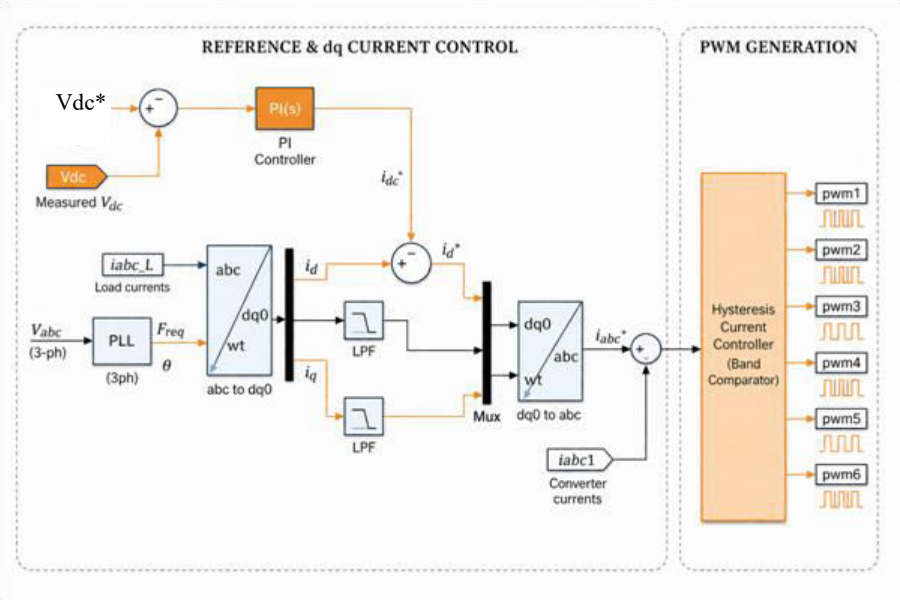

Fig. 8. Control Structure of Shunt Compensator

VI. Simulation Results and Discussion

The proposed grid-connected photovoltaic system using a SEPIC–Ćuk based bipolar DC-link transformerless inverter is analyzed under varying solar irradiation conditions in MATLAB/Simulink. The purpose of this simulation is to study the dynamic response of the PV system, inverter, load, and grid when solar power gradually decreases. In the simulated system, the PV array initially generates sufficient power to supply the connected load and also export the excess power to the utility grid as shown in Fig.9. As the solar irradiation level decreases, the PV output power reduces accordingly, and the grid automatically compensates for the power deficit to maintain continuous supply to the load. Finally, when the solar irradiation becomes zero, the PV system stops generating power and the grid alone supplies the entire load demand. In this analysis, the solar irradiation is varied over a simulation time of 1 second. From 0 to 0.2 s, the irradiation is maintained at 1000 W/m², representing standard operating condition. During this interval, the PV array produces maximum output power, the DC-link voltage remains stable, and the inverter injects active power into the grid while also feeding the local load. From 0.2 to 0.4 s, the irradiation decreases from 1000 W/m² to 800 W/m², causing a slight reduction in PV voltage and current, and therefore a

reduction in generated power. However, the load continues to receive uninterrupted power because the grid starts contributing a small additional amount of power. From 0.4 to 0.6 s, the irradiation further decreases from 800 W/m² to 500 W/m², which results in a more noticeable drop in PV output power. Consequently, the power delivered to the grid decreases, while the grid-side power drawn by the load increases. From 0.6 to 0.8 s, the solar irradiation is reduced from 500 W/m² to 300 W/m². Under this condition, PV generation becomes significantly low, and most of the load demand is supported by the grid. The inverter control maintains synchronization with the grid and ensures smooth transition of power sharing between the PV source and utility supply. During the interval 0.8 to 1.0 s, the irradiation falls from 300 W/m² to 0 W/m². At this stage, the PV output power gradually approaches zero, and the grid fully takes over the supply of load power. This confirms that the proposed system can maintain reliable load operation even under complete absence of solar energy. The simulation results clearly show that the PV power is directly dependent on solar irradiation. When irradiation is high, the PV system supplies both the load and the grid. As irradiation decreases, the PV contribution reduces, and the grid import increases automatically. When irradiation becomes zero, the grid acts as the sole source of power for the load. This demonstrates the effectiveness of the proposed control strategy in maintaining power balance under varying environmental conditions. The DC-link voltage remains regulated, the inverter output remains synchronized with the grid, and the load voltage is maintained nearly constant throughout the simulation. The power flow behavior validates the proper coordination between the PV system and the utility grid.

The active power balance of the system can be expressed as

$$P_{PV} + P_{Grid} = P_{Load} \tag{30}$$

when the PV power is only used for load support, and as

$$P_{PV} = P_{Load} + P_{Export} \tag{31}$$

when the PV generation exceeds the load demand and excess power is injected into the grid. Under zero irradiation condition,

$$P_{PV} = 0 \tag{32}$$

Therefore,

$$P_{Grid} = P_{Load} \tag{33}$$

This confirms that the grid compensates for the reduction in solar generation and guarantees continuous power supply to the load.

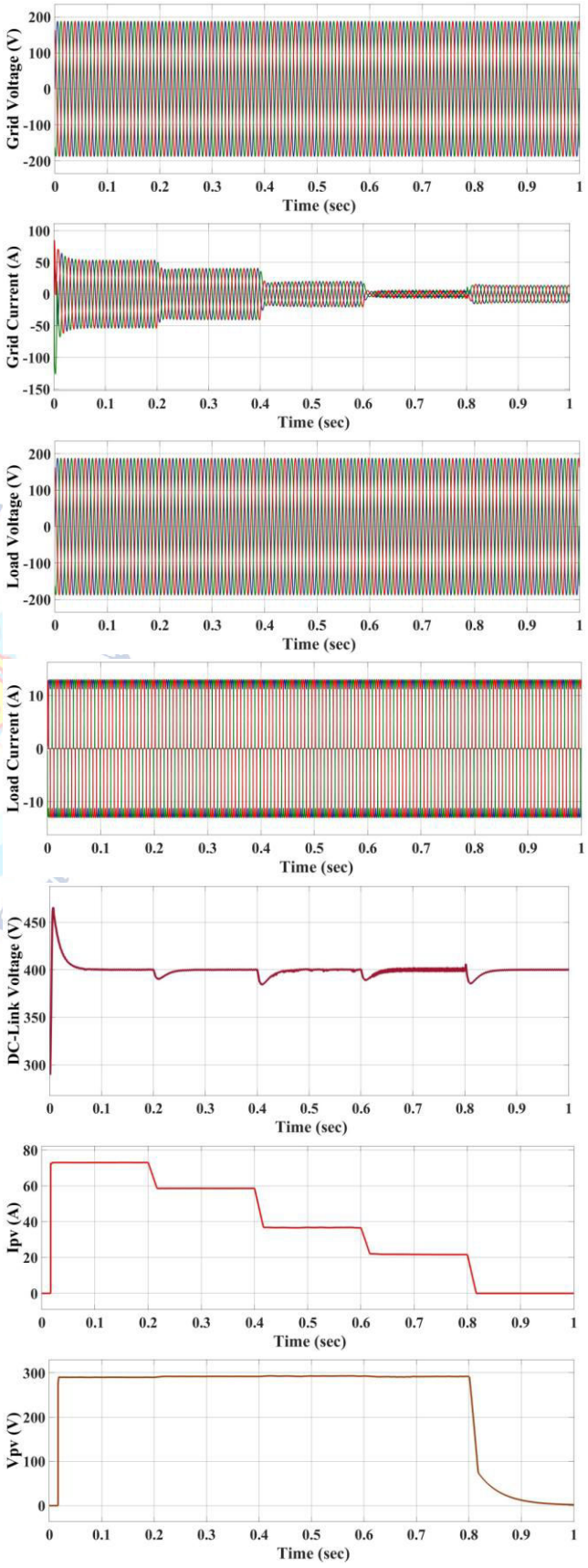

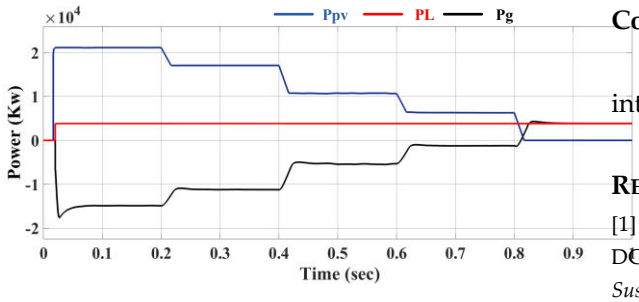

Fig.9 Simulation results of Grid-Connected PV System Under Varying Solar Irradiation

Conclusion

This paper presented a SEPIC–Ćuk based bipolar DC-link transformerless inverter for grid-connected photovoltaic (PV) systems, aimed at improving overall power quality and system performance. The proposed topology effectively combines the advantages of SEPIC and Ćuk converters to achieve flexible voltage conversion with reduced ripple and enhanced voltage regulation. The integration of a bipolar DC-link structure enables balanced voltage distribution and significantly reduces common-mode leakage current, thereby improving the safety and reliability of transformerless operation. The elimination of the transformer contributes to reduced system cost, size, and power losses, resulting in improved efficiency and higher power density. The implemented control strategy, based on maximum power point tracking (MPPT) and grid synchronization, ensures optimal energy extraction from the PV system and stable interaction with the utility grid. Additionally, the use of advanced current control techniques enables effective compensation of harmonics and reactive power, leading to improved power factor and reduced total harmonic distortion (THD). Simulation results validate the effectiveness of the proposed system under varying solar irradiance conditions. The results demonstrate that the system maintains stable DC-link voltage, delivers sinusoidal grid currents, and achieves significant improvement in power quality parameters. Overall, the proposed SEPIC–Ćuk based bipolar DC-link inverter provides a reliable, efficient, and cost-effective solution for modern grid-connected PV systems, making it highly suitable for future renewable energy applications and smart grid integration.

Conflict of interest statement

Authors declare that they do not have any conflict of interest.

REFERENCES

[1] J. J. Justo, F. Mwasilu, J. Lee, and J. W. Jung, "AC-microgrids versus DC-microgrids withy distributed energy resources: A review," *Renew. Sustainable Energy Rev.*, vol. 24, pp. 387–405, 2013.

[2] H. Kakigano, Y. Miura, and T. Ise, "Low-voltage bipolar-type DC microgrid for super high quality distribution," *IEEE Trans. Power Electron.*, vol. 25, no. 12, pp. 3066–3075, Dec. 2010.

[3] J. C. Vasquez, J. M. Guerrero, J. Miret, M. Castilla, and L. Vicu˜na, "Hierarchical control of intelligent microgrids," *IEEE Ind. Electron. Mag.*, vol. 4, no. 4, pp. 23–29, Dec. 2010.

[4] S. R. Huddy and J. D. Skufca, "Amplitude death solutions for stabilization of DC microgrids with instantaneous constant-power loads," *IEEE Trans. Power Electron.*, vol. 28, no. 1, pp. 247–253, Jan. 2013.

[5] H. Kakigano, Y. Miura, and T. Ise, "Distribution voltage control for DC microgrids using fuzzy control and gain-scheduling technique," *IEEE Trans. Power Electron.*, vol. 28, no. 5, pp. 2246–2258, May 2013.

[6] J. Lago, J. Moia, and M. L. Heldwein, "Evaluation of power converters to implement bipolar dc active distribution networks—DC–DC converters," in *Proc. Energy Convers. Congr. Expo.*, 2011, pp. 985–990.

[7] R.-J. Wai and K.-H. Jheng, "High-efficiency single-input multiple-output DC–DC converter," *IEEE Trans. Power Electron.*, vol. 28, no. 2, pp. 886– 898, Feb. 2013.

[8] P. Patra, A. Patra, and N. Misra, "A single-inductor multiple-output switcher with simultaneous buck, boost and inverted outputs," *IEEE Trans. Power Electron.*, vol. 27, no. 4, pp. 1936–1951, Apr. 2012.

[9] X. Yu, K. Jin, and Z. Liu, "Capacitor voltage control strategy for halfbridge three-level DC/DC converter," *IEEE Trans. Power Electron.*, vol. 29, no. 4, pp. 1557–1561, Apr. 2014

[10] E. Landsman, "A unifying derivation of switching DC-DC converter topologies," in *Proc. IEEE Power Electron. Spec. Conf.*, PESC1979, pp. 239–243.

[11] D. Maksimovic and S. Cuk, "General properties and synthesis of PWM DC-to-DC converters," in *Proc. IEEE Power Electron. Spec. Conf.*, PESC1989, pp. 515–525.

[12] E. Duran, M. Sidrach-de-Cardona, J. Galan, and J. M. Andujar, "Comparative analysis of buck-boost converters used to obtain I–V characteristic curves of photovoltaic modules," in *Proc. IEEE Power Electron. Spec. Conf.*, 2008, pp. 2036–2042.

[13] B. R. Lin and F. Y. Hsieh, "Soft-switching Zeta-flyback converter with a buck-boost type of active clamp," *IEEE Trans. Ind. Electron.*, vol. 54, no. 5, pp. 2813–2822, Oct. 2007.

[14] S. S. Ghosh, K. S. Nathan, Y. P. Siwakoti, *et al.*, "Dual polarity DC–DC converter integrated grid-tied singlephase transformer less inverter for solar application," *The Journal of Engineering*, vol. 2019, no. 17, pp. 3962-3966, 2019.

[15] K. Nathan *et al.*, "Benefits of the Coupled Inductors Combined Cuk-SEPIC (CI-CCS) Converter," *The Journal of Engineering*, 2018.

[16] M. B. Ferrera, S. P. Litran, E. D. Aranda, *et al.*, "A converter for bipolar DC link based on SEPIC-Cuk combination," *IEEE Trans. Power Electron.*, vol. 30, no. 12, pp. 6483-6487, 2015.

[17] B.-R. Lin, K.-L. Shih, J.-J. Chen, *et al.*, "Implementation of a zero voltage switching Sepic-Cuk converter," in *2008 3rd IEEE Conference on Industrial Electronics and Applications*, 2008: IEEE, pp. 394-399.
[18] A. Anand and B. Singh, "Power factor correction in Cuk–SEPIC-based dual-output-converter-fed SRM drive," *IEEE Trans. Ind. Electron.*, vol. 65, no. 2, pp. 1117-1127, 2017.
[19]K.Nathan, S. Ghosh, Y. Siwakoti, *et al.*, "A New DC–DC Converter for Photovoltaic Systems: Coupled-Inductors Combined Cuk-SEPIC Converter," *IEEE Trans. Energy Convers.*, vol. 34, no. 1, pp. 191-201, 2018.
[20] J. Wang, J. D. Yan, L. Jiang, *et al.*, "Delay-dependent stability of single-loop controlled grid-connected inverters with LCL filters," *IEEE Trans. Power Electron.*, vol. 31, no. 1, pp. 743-757, Jan. 2016.
[21] S.-K. Chung, "Phase-locked loop for grid-connected three-phase power conversion systems," *Proc. Inst. Elect. Eng.-Electron. Power Appl.*, vol. 147, no. 3, pp. 213-219, 2000.